Physics in Medicine & Biology

IPEM Institute of Physics and Engineering in Medicine

RECEIVED
6 May 2020

REVISED
12 November 2020

ACCEPTED FOR PUBLICATION
2 December 2020

PUBLISHED
29 January 2021

PAPER

A method using 4D dose accumulation to quantify the interplay effect in lung stereotactic body radiation therapy

Carlos Huesa-Berral[1,2], **Javier Burguete**[1], **Marta Moreno-Jiménez**[3] **and Juan Diego Azcona**[2]

[1] Department of Physics and Applied Mathematics, School of Sciences, Universidad de Navarra. C/ Irunlarrea, E-31008 Pamplona, Navarra, Spain
[2] Service of Radiation Physics and Radiation Protection, Clínica Universidad de Navarra, Avda. Pío XII, E-31008 Pamplona, Navarra, Spain
[3] Service of Radiation Oncology, Clínica Universidad de Navarra, Avda. Pío XII, E-31008 Pamplona, Navarra, Spain

E-mail: jazcona@unav.es

Keywords: deformable image registration, interplay effect, 4D dose accumulation

Abstract

The purpose of this study was to devise and evaluate a method to quantify the dosimetric uncertainty produced by the interplay between the movement of multileaf collimator and respiratory motion in lung stereotactic body radiation therapy. The method calculates the dose distribution for all control points from a dynamic treatment in all respiratory phases. The methodology includes some characteristics of a patient's irregular breathing patterns. It selects, for each control point, the phases with maximum and minimum mean dose over the tumor and their corresponding adjacent phases, whenever necessary. According to this selection, the dose matrices from each control point are summed up to obtain two dose distributions in each phase, which are accumulated in the reference phase subsequently by deformable image registration (DIR). D_{95} and $D_{\mathrm{min},0.035cc}$ were calculated over those accumulated dose distributions for Gross Tumor Volume (GTV), Planning Target Volume—based on Internal Target Volume approach—and Evaluation Target Volume (ETV), a novel concept that applies to 4D dose accumulation. With the ETV, DIR and interplay uncertainties are separated. The methodology also evaluated how variations in the breathing rate and field size affects the mean dose received by the GTV. The method was applied retrospectively in five patients treated with intensity modulated radiotherapy—minimum area defined by the leaves configuration at any control point was at least 4 cm^2. Uncertainties in tumor coverage were small (in most patients, changes on D_{95} and $D_{\mathrm{min},0.035cc}$ were below 2% for GTV and ETV) but significant over- and under-dosages near ETV, which can be accentuated by highly irregular breathing. Uncertainties in mean dose for GTV tended to decrease exponentially with increasing field size and were reduced by an increase of breathing rate. The implementation of this method would be helpful to assess treatment quality in patients with irregular breathing. Furthermore, it could be used to study interplay uncertainties when small field sizes are used.

1. Introduction

A patient's respiration during radiotherapy for a lung tumor induces motion and deformation of the tumor and this is a cause of uncertainty in calculation and delivery of the dose (Keall *et al* 2006, Brock *et al* 2017, Schwarz *et al* 2017, Yang and Timmerman 2018). Furthermore, in dynamic treatment techniques such as intensity modulated radiotherapy (IMRT) and volumetric modulated arc therapy tumor movement may interact with the dynamic radiation field—the so-called interplay effect (Bortfeld *et al* 2002)—resulting in differences between the planned dose and the delivered dose (Bortfeld *et al* 2004, Keall *et al* 2006, Court *et al* 2008). In accordance with the definition of the interplay effect, these dosimetric variations depend on patient- and machine-specific parameters, such as, field size, amplitude of organ motion, respiratory rate, asymmetry of the respiratory cycle and dose rate. Bortfeld *et al* (2004) showed that after a long series of fractions the interplay effect is negligible.

However, in stereotactic body radiation therapy (SBRT) it may be a concern because SBRT is typically hypofractionated. Several studies (Court *et al* 2010, Ong *et al* 2011, Edvardsson *et al* 2018, Netherton *et al* 2018) have demonstrated that the dosimetric effect of interplay generally increases with increasing plan complexity. The authors of two of these studies (Edvardsson *et al* 2018, Netherton *et al* 2018) recommend reduction of the number of monitor units (MU) per Gy in order to mitigate the interplay effect.

In the case of lung SBRT, the quantification of dosimetric uncertainty due to the interplay effect is complex because the uncertainty depends on all of the specific parameters mentioned above. The research in this area is summarized in two reviews (Schwarz *et al* 2017, Yang and Timmerman 2018). Several retrospective studies of lung SBRT patients treated by dynamic techniques have been carried out (Rao *et al* 2012, Sterpin *et al* 2012, Li *et al* 2013, Wanet *et al* 2014, Zou *et al* 2014). The approach used to quantify the interplay effect in these studies has two parts. First, each control point is synchronized sequentially with the corresponding phase of the respiratory cycle, and consequently each phase has a corresponding dose distribution. Second, a 4D dose distribution in the reference phase is calculated using deformable image registration (DIR) from the dose distributions obtained in the first part. In this way, the 4D dose distribution is calculated taking tumor motion and deformation into account.

The general consensus of these works (Rao *et al* 2012, Sterpin *et al* 2012, Li *et al* 2013, Wanet *et al* 2014, Zou *et al* 2014) is that the interplay effect is negligible. However, all of the authors point out that synchronization of the control points with the corresponding respiratory phases was carried out under the assumption that a patient's breathing was regular. Could irregular respiratory motion also be a source of dosimetric errors? Mutaf *et al* (2011) conducted a simulation study of the dosimetric impact of irregular respiratory motion. They simulated irregular respiratory cycles modifying only the amplitude, and found that systematically irregular respiratory motion—for example, when the tumor motion determined at the planning step is systematically less than the mean tumor motion during the treatment—could indeed result in dosimetric errors of potential clinical significance. A study by Riley *et al* (2014) in gated treatments confirmed that clinically relevant dosimetric uncertainties could be observed with irregular respiratory motion. Moreover, other studies (Court *et al* 2008, 2010, Ong *et al* 2011, 2013, Stambaugh *et al* 2013, Edvardsson *et al* 2018) used phantoms to indicate that dosimetric uncertainties due to the interplay effect generally increase with long breathing periods.

Irregular breathing in this paper refers to any circumstance that can alter the synchronization between the sequence of control points and the phases of the ideal regular respiratory cycle (the one obtained from the 4D CT). Under this definition, at least one of the following parameters varies in the respiratory pattern: (i) the amplitude (as characterized in the 4D CT), (ii) the frequency (i.e. the breathing rate is not constant), (iii) the waveform. (i.e. respiratory pattern shape changes between periods) and (iv) the synchronization among the control points and the respiratory pattern during the treatment (i.e. coughing). We would like to note that this last point covers other processes that, although not strictly due to irregular breathing, could lead to a loss of synchronization, as for example the beam off time during leaves motion or gantry rotation (only in IMRT delivery). Previous studies mentioned above (Rao *et al* 2012, Sterpin *et al* 2012, Li *et al* 2013, Wanet *et al* 2014, Zou *et al* 2014) assumed regular breathing to assign control points to respiratory phases, so the variation of the points (i), (ii) and (iii) were not included. In addition to this, they assigned consecutive control points to consecutive respiratory phases. Then, a variation of (iv) was not included either. Unlike those studies, our method is able to assign control points to respiratory phases including the variation of two parameters: the frequency and the synchronization. We assume that 4DCT represents properly the tumor motion and that the position of the tumor at any time can be properly resolved by any of the closest breathing phases. Therefore, a variation of the amplitude and the waveform is restricted to the limitations of the 4DCT. However, uncertainty in breathing amplitude during the treatment is small for most patients (Bissonnette *et al* 2009, Sonke *et al* 2009).

The novelty of this work is to present a general method to evaluate the interplay effect on the tumour coverage due to a specific treatment plan designed using the actual patient's respiratory information available on their planning 4D CT. We have developed a method that, taking into account the interplay effect in SBRT plans, estimated the upper and lower limit for the potential dose received by a tumor. We determine these limits in the Gross Tumor Volume (GTV) and in the Planning Target Volume (PTV). In addition, we estimate the error margins in the Evaluation Target Volume (ETV)—a novel concept proposed by our group (Azcona *et al* 2019)—to be applied to 4D accumulated dose distributions. It considers an expansion from GTV taking into account the delineation, patient setup and imaging, and dose delivery uncertainties, such as PTV, plus the geometrical uncertainties in DIR. It is used to identify whether the dosimetric uncertainties produced in PTV due to the interplay effect after dose accumulation are clinically relevant. This is because the concept of PTV has shortcomings when applied to 4D accumulated dose distributions.

We have also investigated the relationship between the dosimetric uncertainty that interplay induces in tumour coverage and the previously-established patient- and machine-specific parameters. In particular, our method can be applied to study the behaviour of the interplay effect when breathing rate and field size is varied.

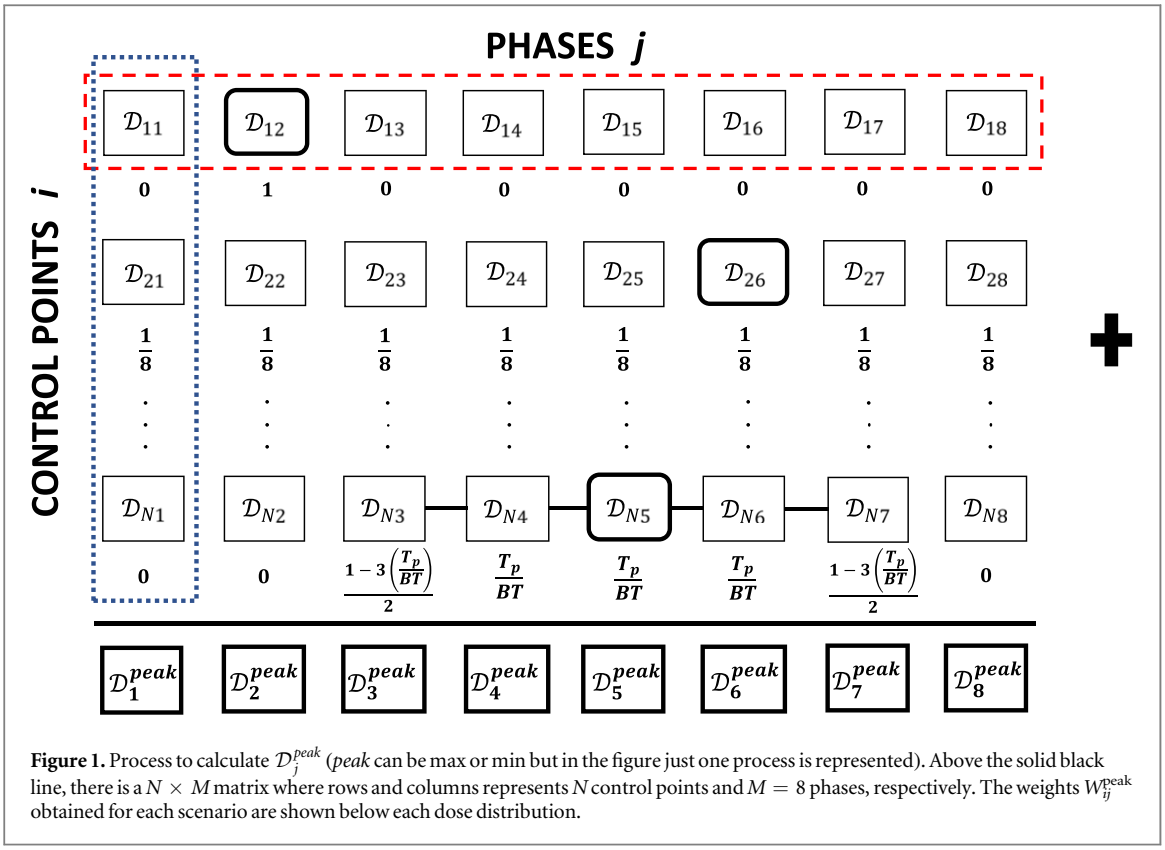

Figure 1. Process to calculate $\mathcal{D}_j^{peak}$ (*peak* can be max or min but in the figure just one process is represented). Above the solid black line, there is a $N \times M$ matrix where rows and columns represents N control points and $M = 8$ phases, respectively. The weights W_{ij}^{peak} obtained for each scenario are shown below each dose distribution.

These results, obtained for different breathing patterns, were put in connection with the minimum field size used in treatment planning of the clinical cases presented.

2. Material and methods

2.1. Description of the method

The essence of our approach is to determine the dose distributions with the maximum and minimum mean dose that, as a consequence of the interplay effect, would potentially be received by a tumor (in the text, these dose distributions will be called: the *maximum* and the *minimum potential dose distributions*). To include any possible variation of the breathing rate and the synchronization during the treatment, our method is not restricted to assign successive control points to contiguous respiratory phases. As we noted previously, the possible variations of the amplitude and the waveform can be taking into account under the limitations of the 4DCT.

The whole method is represented in figure 1. The method requires calculation of the dose distributions $\mathcal{D}_{ij}$ for each control point i on all breathing phases j. Because N is the number of control points of a treatment plan and M is the number of breathing phases, the method works with $N \times M$ dose distributions $\mathcal{D}_{ij}$ (figure 1, all such dose distributions are represented as a black square).

For each control point on each phase of 4DCT, we evaluate the mean dose over the GTV. The phases for which the mean dose are maximum and minimum are selected for each control point i (the red dashed rectangle in figure 1 represents the dose distributions when $i = 1$, and the black curved square indicates the selected dose distribution for each control point). Once this selection has been done for every control point, the method evaluates whether the control points are active during several phases or not. To accommodate these considerations, we apply a process to assign weights between 0 and 1 to each control point in all phases. This is done by comparing the beam-on time (BT) with the period of the respiratory cycle. The BT is defined as $BT = \frac{MU}{DR}$, where MU and DR represent the monitor units of a control point and the dose rate, respectively. The period of the respiratory cycle, represented by T and with the phase time, which is defined as $T_p = \frac{T}{M}$. There are three outcomes from this comparison: $BT < T_p$, $BT > T$ and $T_p < BT < T$.

- For $BT < T_p$, the control point i will be active in one phase. Thus, only the selected phase for which the mean dose over GTV is maximum or minimum will be weighted with a weight of 1; the rest of phases will be weighted with 0. In figure 1, this case is represented in the first row.

- For $BT > T$, the control point i will be active in all phases j. We assume all phases will have the same weights: $\frac{1}{M}$. In figure 1, this case is represented in the second row.
- For $T_p < BT < T$, the control point i will be active during various phases, i.e. this control point i is administered around the phase selected for which the mean dose over GTV is maximum or minimum. The number of phases where this control point is active can be obtained through $q = \frac{BT}{T_p}$. So, the weighting will be $\frac{T_p}{BT}$ for the phase selected previously and for its $m = \left\lfloor \frac{q-1}{2} \right\rfloor$ adjacent phases on each side (note that $\lfloor \rfloor$ stands for rounding to the lower integer). The remaining weight, if any, will be assigned to the other phases with a value $\frac{1-(2m+1)\frac{T_p}{BT}}{2}$. All other phases will be weighted with 0. In figure 1, this case is represented in the Nth row.

Finally, two dose matrices are obtained for each phase j, denoted as $\mathcal{D}_j^{\max}$ and $\mathcal{D}_j^{\min}$, respectively (this process is highlighted by blue dotted rectangle for the phase $j = 1$ in figure 1 and the dose matrices mentioned are represented by squares below the solid line). They are obtained by summing up $\mathcal{D}_{ij}$ taking into account the weights assigned to each control point i. The weights assigned to each control point in all phases described above are represented as $W_{ij}^{\max}$ and $W_{ij}^{\min}$ (these weights are displayed in figure 1 below each point in the matrix for the three examples shown):

$$\mathcal{D}_j^{\max} = \sum_{i=1}^{N} \mathcal{D}_{ij} W_{ij}^{\max}, \tag{1}$$

$$\mathcal{D}_j^{\min} = \sum_{i=1}^{N} \mathcal{D}_{ij} W_{ij}^{\min}. \tag{2}$$

In this way, $\mathcal{D}_j^{\max}$ and $\mathcal{D}_j^{\min}$ correspond to dose matrices for each phase j that maximize and minimize the mean dose received by GTV.

The last step of the method consists in accumulating, by DIR, the phase dose matrices $\mathcal{D}_j^{\max}$ and $\mathcal{D}_j^{\min}$ onto the reference phase in order to obtain maximum and minimum potential accumulated dose distributions that estimate the upper and lower error margins in the administration of a SBRT dose. These accumulated dose distributions are represented by $\mathcal{D}_{acc}^{\max}$ and $\mathcal{D}_{acc}^{\min}$, respectively. To carry out this procedure, we used the commercial software MIM (MIM Software Inc., Cleveland, OH), which was validated for dose accumulation by DIR in a previous work by our group (Azcona *et al* 2019). From these dose distributions, dosimetric indicators for the GTV, the PTV and the ETV are calculated.

2.2. Treatment planning

To evaluate the method and demonstrate its functionality, we applied the method for five patients with lung tumors treated with SBRT. These patients were scanned in a Siemens Somatom Plus CT while their respiratory signal was collected through a Sentinel 4DCT (C-RAD, Uppsala, Sweden), an optical tracking system that provides an external signal to the CT to sort the raw data according to the respiratory phases. Sorting is done by *phase binning*: the respiratory cycle is divided into eight phases of equal duration, and the 3D CTs are assigned to one of the eight different phases. In this way, a 4D CT is obtained.

The GTV was delineated in each respiratory phase of the 4D CT. The Internal Target Volume (ITV) that encompasses the GTVs from all respiratory phases was generated, and a PTV was created by adding, to the ITV, a margin of 3 mm in anterior-posterior and lateral directions, and 5 mm in the superior-inferior direction (these margins can be modified by the medical doctor for treatment planning purposes). No density override was done in the ITV-to-PTV expansion. Both ITV and PTV were built in the reference phase. The IMRT plans were created in Pinnacle v9.10 with a 4D CT, using the collapsed cone convolution as the dose calculation algorithm. The dose calculation grid resolution in each spatial direction was 2 mm. The IMRT plans were generated for an Elekta Versa linear accelerator (LINAC) using direct machine parameter optimization (DMPO), which allows the user to control the minimum beam aperture. DMPO optimization was done over the tumor volumes depicted in the reference phase of the 4D CT. We have also specified a 4 cm^2 area as minimum area at any control point in the sequence. With this selection we expected our treatment plans to be robust under interplay effect. We will check with our algorithm that this was, in fact, the case. Patients were treated in 3, 5, or 8 fractions, with prescribed doses up to 51.3–52 Gy, 56.5, and 63.3 Gy, respectively, according to three different SBRT protocols depending on the size and location of the tumor. Table 1 includes clinical data for each patient and treatment planning characteristics.

From the Dose Volume Histogram (DVH), two dosimetric indicators were determined to assess the tumor volume (GTV and PTV coverage): D_{95} and $D_{\min,V}$. The latter indicator estimates the minimum dose to the tumor without taking into account the $V = 0.035$ cm^3 with minimum dose values. But the PTV has a drawback when evaluating these indicators on accumulated doses: cold points can be obtained because the DIR removes

Table 1. Patients with their tumor motion, average breathing period of respiratory cycle, number of fields and control points used in treatment and the voxel resolution in 4D CT. The GTV mean volume is defined as the mean volume of the tumor as it is delimited in each phase. Breathing period was obtained from the respiratory signal (collect by Sentinel 4DCT (C-RAD, Uppsala, Sweden)), which was post-processed by our code in Matlab.

Pat. #	GTV motion amplitude (mm)			GTV volume (cm^3)		# Fields	# Control points	Breathing period: $T(s)$		Resolution (mm^3)
	LAT	AP	SI	Mean	STD			Mean	STD	
1	1.0	1.5	4.8	4.45	0.53	9	27	3.04	0.8	0.97 × 0.97 × 2.1
2	0.8	2.0	12.5	1.37	0.25	7	27	3.12	0.12	0.96 × 0.96 × 2.1
3	0.6	4.1	4.1	2.80	0.45	8	29	6.70	3.32	0.92 × 0.92 × 2.1
4	1.7	3.7	4.8	0.99	0.17	9	19	3.48	1.03	0.96 × 0.96 × 2.1
5	1.0	1.1	1.3	5.99	0.34	8	28	3.10	0.19	0.96 × 0.96 × 2.1

respiratory motion during the accumulation process, while the breathing tumor movement is retained in the PTV as it is expanded from the ITV. So, these metrics were also used to evaluate the dose distributions in a different target volume, called ETV (Azcona *et al* 2019). The ETV is used to assess uncertainties in the GTV after 4D dose accumulation using DIR, in order to better understand the dosimetric uncertainties due to motion and deformation. The ETV is expanded from the GTV and includes: (1) DIR uncertainty, by computing the target registration error on 50 pairs of landmarks set by an expert medical doctor on the lung that contained the tumor (Azcona *et al* 2019); (2) the interobserver GTV delineation uncertainty and (3) the setup, including image registration uncertainty plus dose delivery uncertainties. The ETV is a new volume definition to include the usual uncertainties (2) and (3) plus the one induced by the accumulation (1). As the ETV is defined on the basis (as an expansion) of the GTV, the interobserver variation in the determination of GTV must be included in the ETV. It is very important to note that the ETV is used for dose evaluation over 4D accumulated dose distributions, and should be always expanded from the GTV as depicted in the phase in which 4D dose is accumulated. The effect of motion is absorbed in the DIR. The PTV, on the contrary, is used for planning and evaluating over 3D dose distributions, and its expansion explicitly includes tumor motion (i.e. expansion is done from the ITV). In general, ETV is smaller than PTV, although under certain circumstances, as for example when tumor motion is due to important deformations in GTV or PTV modifications due to treatment planning purposes, ETV could be larger than PTV. In-house computer code was programmed in MATLAB to calculate these indicators.

2.3. Assessment of uncertainties in tumor coverage: dosimetric indicators

In the current work, we compare 4D dose distributions with and without interplay thereby isolate more clearly the uncertainties due to the interplay effect from the uncertainties due to the accumulation effect.

For this purpose, three dose matrices were used to evaluate tumor coverage: the accumulated dose from the 4DCT without taking into account the interplay effect and denoted as $\mathcal{D}_{acc}$ and the dose distributions obtained through the method proposed in this paper, $\mathcal{D}_{acc}^{\max}$ and $\mathcal{D}_{acc}^{\min}$. From these three dose matrices, the dosimetric indicators D_{95} and $D_{\min,V}$ were obtained for the GTV, PTV and ETV, in the reference phase. To refer to these indicators, we use the notation $D_{95}^{TV}(\mathcal{D})$ and $D_{\min,V}^{TV}(\mathcal{D})$, where $\mathcal{D}$ is the accumulated dose distribution from which the indicators have been calculated on the corresponding target volume TV (GTV, PTV or ETV). With these indicators, we quantified the differences between $\mathcal{D}_{acc}$ with $\mathcal{D}_{acc}^{\max}$ and $\mathcal{D}_{acc}^{\min}$ on a target volume TV.

Quantification of the dosimetric uncertainties produced on a target volume TV by the interplay effect is calculated using:

$$\Delta D_{95}^{TV} = \max\{|D_{95}^{TV}(\mathcal{D}_{acc}) - D_{95}^{TV}(\mathcal{D}_{acc}^{\max})|, |D_{95}^{TV}(\mathcal{D}_{acc}) - D_{95}^{TV}(\mathcal{D}_{acc}^{\min})|\}, \tag{3}$$

$$\Delta D_{\min,V}^{TV} = \max\{|D_{\min,V}^{TV}(\mathcal{D}_{acc}) - D_{\min,V}^{TV}(\mathcal{D}_{acc}^{\max})|, |D_{\min,V}^{TV}(\mathcal{D}_{acc}) - D_{\min,V}^{TV}(\mathcal{D}_{acc}^{\min})|\}, \tag{4}$$

where ΔD_{95}^{TV} and $\Delta D_{\min,V}^{TV}$ represent the dosimetric uncertainties due to the interplay effect that arise in the indicators D_{95} and $D_{\min,V}$ for the volume TV (GTV, PTV or ETV).

In addition, for each control point i among all phases j, we also calculated the average of the mean dose over the GTV superimposed onto $\mathcal{D}_{ij}$:

$$\overline{D}_i = \frac{\sum_{j=1}^{M}\langle\mathcal{D}_{ij}\rangle_{GTV}}{M}, \tag{5}$$

where $\langle\cdot\rangle_{GTV}$ denotes the spatial average over the GTV.

2.4. Assessment of dosimetric uncertainties due to breathing rate

To quantify the effect of breathing on dosimetric uncertainties, we related different breathing rates to the dose received by the GTV.

Using the method proposed in 2.1, we have calculated the dose distributions $\mathcal{D}_{acc}^{\max}$ and $\mathcal{D}_{acc}^{\min}$ at specific frequencies: $\frac{f}{4}$, $\frac{f}{2}$, f, $2f$, $4f$, where f is the patient's normal breathing rate. For each pair of $\mathcal{D}_{acc}^{\max}$ and $\mathcal{D}_{acc}^{\min}$, we obtain the corresponding GTV DVHs.

The correlation between breathing rate (over the range of frequencies $\left[\frac{f}{4}, 4f\right]$) and the corresponding GTV DVHs shows how the variation of breathing rate affects interplay effect.

2.5. Assessment of dosimetric uncertainties due to field size

Partial irradiation combined with motion produces uncertainty in the mean dose absorbed at each of the voxels pertaining to the tumor volume. In this section, we studied the effect of field size on uncertainty in the mean dose received by GTV.

For a specific control point i, the method calculates $\overline{D_i}$ from equation (5) and the standard deviation of the set of M spatial averages $\langle \mathcal{D}_{ij} \rangle_{GTV}$, denoted as SD_i. In this way, the dosimetric uncertainty for each control point i was interpreted as the coefficient of variation in mean dose, calculated from:

$$CV = \frac{SD_i}{\overline{D_i}}. \tag{6}$$

To evaluate the effect of field size over CV, the method calculates two parameters:

- The field size of control points, represented as A_{cp}, which is defined from the positions of the multi-leaf collimator.
- The mean effective cross-section of the GTV, denoted as A_t. Assuming that the GTV can be approximated by a sphere, A_t is obtained as follows:

$$A_t = \sqrt[3]{\frac{\pi (3V_t)^2}{16}}, \tag{7}$$

where V_t is the mean GTV volume calculated from the patient cohort.

The correlation between CV and the ratio of A_{cp} with A_t shows how the variation of field size affects interplay effect.

In addition, we also quantify the variability of a control point i by the range, denoted as δ_i. We calculate δ_i as the difference between the maximum and minimum $\langle \mathcal{D}_{ij} \rangle_{GTV}$ obtained for a specific control point i.

3. Results

3.1. Tumor coverage: GTV, PTV and ETV metrics

Figure 2 shows the comparison of DVHs between the dose distributions $\mathcal{D}_{acc}$, $\mathcal{D}_{acc}^{\max}$ and $\mathcal{D}_{acc}^{\min}$ for GTV, PTV and ETV. The dosimetric indicators were obtained from these DVHs.

Figure 3 shows the variability due to the interplay effect in the indicators D_{95} and $D_{\min,V}$ calculated for the GTV, PTV and ETV with equations (3) and (4).

The variability in both indicators was small for GTV: for D_{95}, the fluctuations were below 1%; for $D_{\min,V}$, the highest variability was 1.8% in case 3. With regard to the PTV, the uncertainty was also generally small: for D_{95} the highest variability was 1.8%, in case 3; for $D_{\min,V}$, uncertainty was relevant in cases 2 and 3, where the fluctuations were above 5%. The fluctuations in D_{95} and $D_{\min,V}$ calculated on the ETV were small in all cases except case 3, in which D_{95} variation was up to 1.3% and $D_{\min,V}$ variation exceeded 7%.

3.2. Effect of varying the breathing rate

Figure 4 contains results regarding the correlation between breathing frequency and the behaviour of the interplay effect over the GTV. These results were obtained according to the procedure explained in section 2.4, which was carried out for the first two patients of our cohort.

For each frequency, the dosimetric uncertainty can be interpreted as the difference between each pair of DVHs calculated from $\mathcal{D}_{acc}^{\max}$ and $\mathcal{D}_{acc}^{\min}$. For example, for the treatment respiratory frequency f of patients #1 and #2, the difference between D_{95} for $\mathcal{D}_{acc}^{\max}$ and $\mathcal{D}_{acc}^{\min}$ was 0.4 and 0.7 Gy respectively. With both patients there was an inverse correlation between uncertainty and respiratory frequency: as the breathing frequency increased (i.e. as the period of breathing decreased), the difference between DVHs tended to 0.

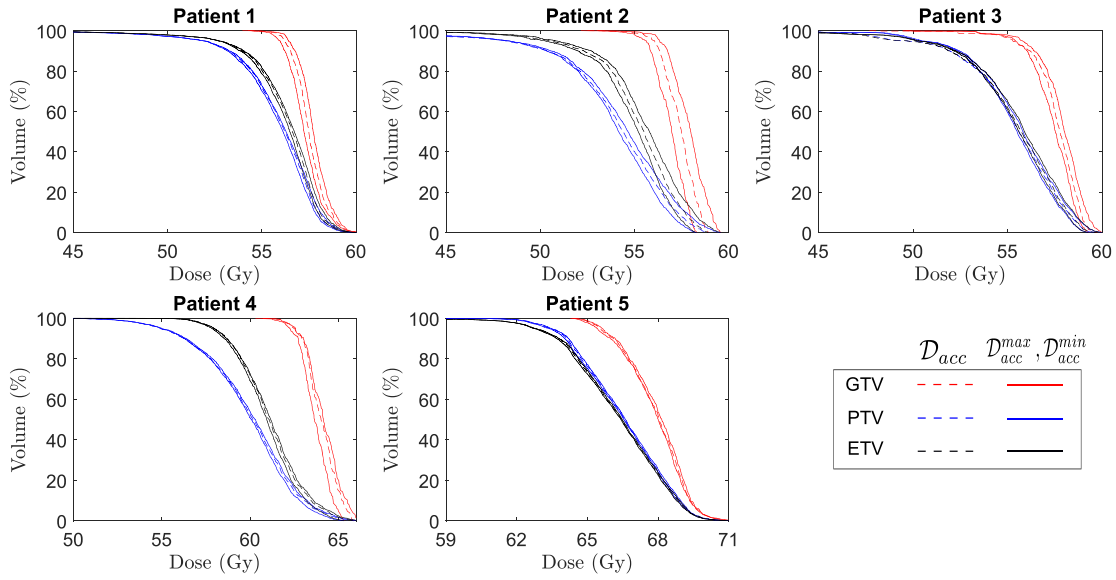

Figure 2. Comparison of DVHs between dose distributions $\mathcal{D}_{acc}$ (dashed line), $\mathcal{D}^{\max}_{acc}$ and $\mathcal{D}^{\min}_{acc}$ (solid line) for GTV(red), PTV (blue) and ETV (black).

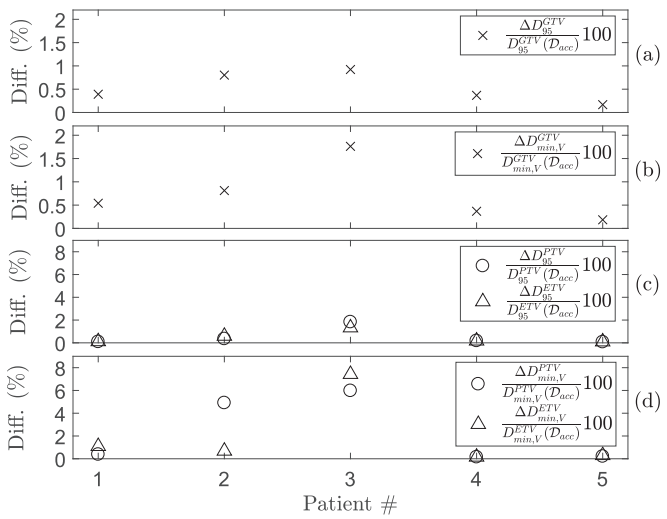

Figure 3. Estimation of variability in dosimetric indicators D_{95} and $D_{\min,V}$ from GTV (panels (a) and (b)), PTV and ETV (panels (c) and (d)) calculated in the reference phase over $\mathcal{D}_{acc}$, $\mathcal{D}^{\max}_{acc}$ and $\mathcal{D}^{\min}_{acc}$, using equations (3) and (4).

3.3. Effect of varying field size

For each control point and for the treatment plan of each patient, figure 5 gives the beam on time (BT) and its corresponding effect on the dose received by the GTV. The top panel shows the beam on time (BT) for control points in all patients, sorted in descending order and divided by each patient's breathing period (T). The second panel shows the mean dose delivered by each control point across all phases ($\overline{D}_i$) in all patients. The third panel shows the range (δ_i) for each control point in all patients. As we discussed, δ_i can be interpreted as the variability of the control point i.

In patient 2, two control points presented variability in delivered dose that was above 0.5 Gy, with a low mean dose ($\overline{D}_{14} = 0.58$ Gy and $\overline{D}_{16} = 0.49$ Gy). The dose variability in the control points in patients 1 and 3 was greater than in the other patients. In patient 1, at least four control points with mean delivered doses greater than 3 Gy, had variability exceeding 0.5 Gy (control points 1 and 5 over 3 Gy and 1 Gy, respectively, with $\overline{D}_1 = 5.41$ Gy and $\overline{D}_5 = 4.1$ Gy). For patient 3, five control points with mean doses delivered above 1 Gy had variability

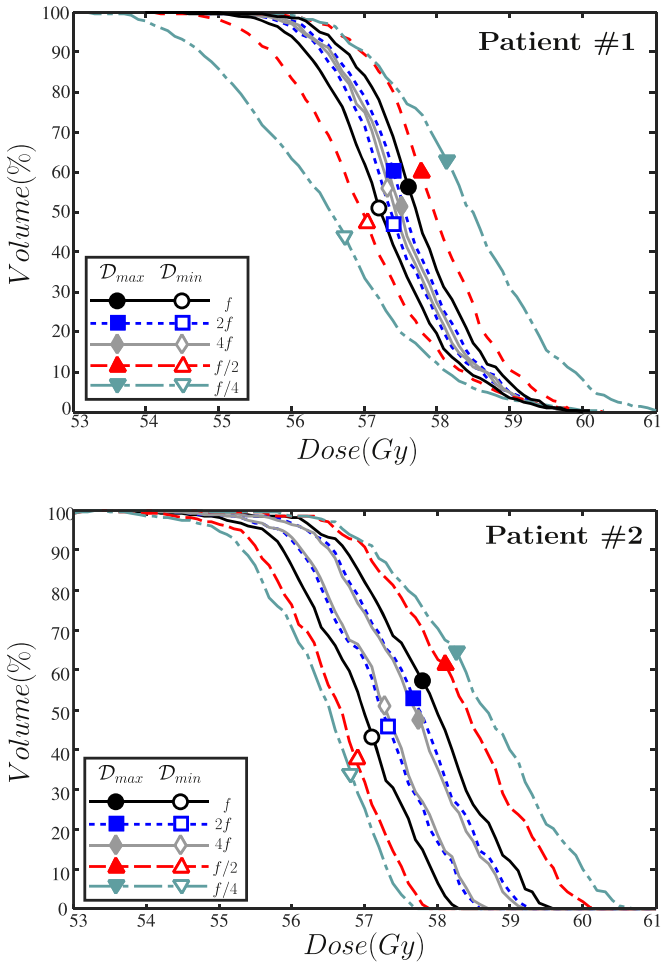

Figure 4. Relationship between breathing rate and the behaviour of interplay effect in GTV. For each frequency, the DVH of GTV is obtained from $\mathcal{D}_{acc}^{\max}$ and $\mathcal{D}_{acc}^{\min}$.

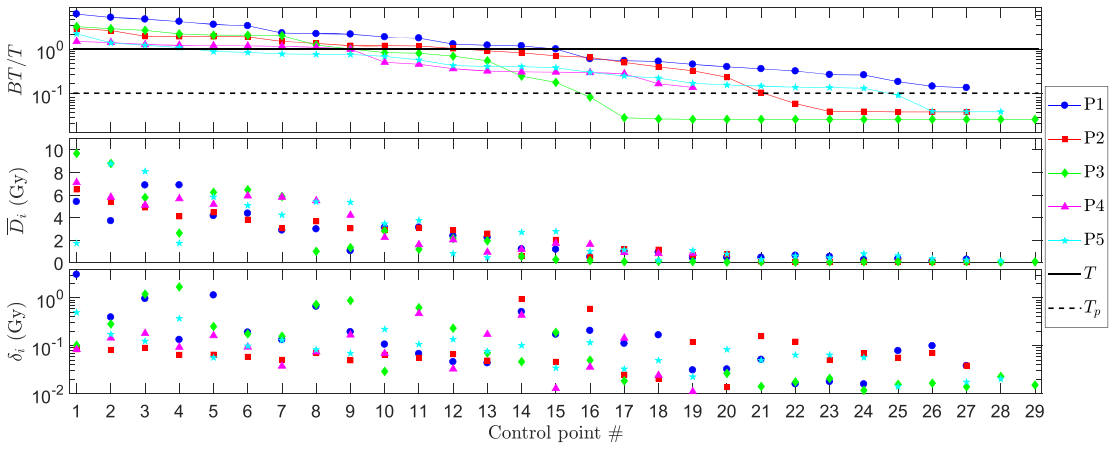

Figure 5. The first panel shows the beam on time (*BT*) for each control point in all patients, divided by their respective period (*T*). The period (*T*) and the phase time (T_p) are represented by a solid and a dashed line, respectively. The second and third panel represent the mean dose administered to the GTV ($\overline{D}_i$) and the range (δ_i) for each control point in all patients. All control points are ordered according to a decreasing beam-on time.

over 0.5 Gy; in particular, delivered doses at control points #3 and #4 with $\overline{D}_3 = 5.78$ Gy and $\overline{D}_4 = 1.70$ Gy varied over 1.20 Gy and 1.70 Gy, respectively. After control point #17 for this patient, $\overline{D}_i$ is negligible.

As explained previously, an important factor in the $\overline{D}_i$ uncertainty is its field size. Considering the dosimetric uncertainty in the mean dose of a control point *i* as *CV*, its correlation with the field size (A_{cp}) and the tumor area

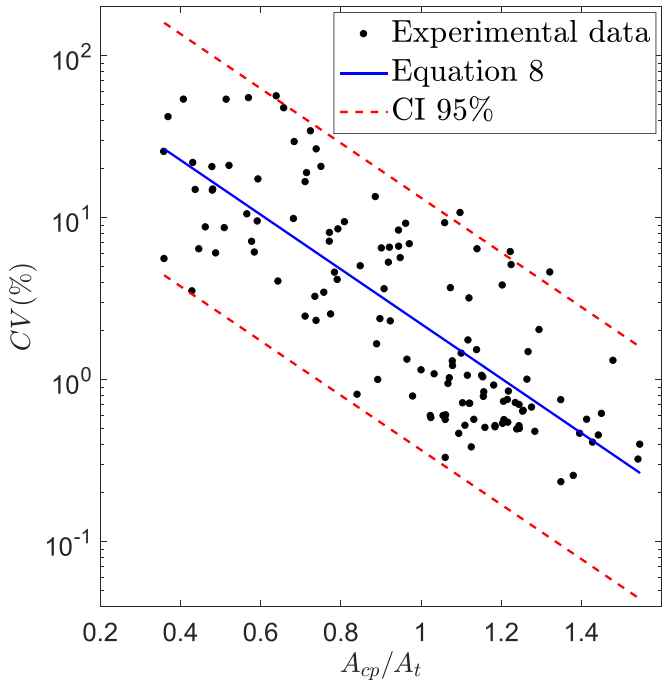

Figure 6. Correlation between the coefficient of variation in mean dose (CV) and the relative tumour area (control point area A_{cp} over mean effective cross-section of the GTV A_t). Solid line: least squares regression fit using equation (8). Dashed lines represent the 95% confidence interval.

(A_t) is shown in figure 6. The correlation shown in the figure is exponential, and we performed a least square linear fit (equation (8)) with $R^2 = 0.64$

$$\log(CV) = -3.88\frac{A_{cp}}{A_t} + 4.67. \tag{8}$$

4. Discussion

4.1. Interplay effect in tumor coverage

With the method proposed in this paper, we have quantified the dosimetric uncertainty in GTV, PTV and ETV that results from the interplay effect. This uncertainty is reflected in the dosimetric indicators (D_{95} and $D_{\mathrm{min},V}$), all of which were calculated over the 4D dose distributions $\mathcal{D}_{acc}$, $\mathcal{D}_{acc}^{\max}$ and $\mathcal{D}_{acc}^{\min}$.

The interplay effect produced dose variations in 4D accumulated doses in the various target volumes. Figure 7 shows the scale of those variations in a sagittal plane: In the first row, (a), where we compare the two 4D dose distributions calculated from the method proposed, there is a hot spot inside the GTV in all cases. The margin of GTV uncertainty due to the interplay effect for dosimetric indicators was generally small in all patients: the highest variability was 1.8% for $D_{\mathrm{min},V}$ in patient 3. These results are in line with other published studies (Rao *et al* 2012, Sterpin *et al* 2012, Li *et al* 2013, Wanet *et al* 2014, Zou *et al* 2014).

The maximization and minimization of the dose over the GTV produces positive and negative differences between $\mathcal{D}_{acc}^{\max}$ and $\mathcal{D}_{acc}^{\min}$ in the lower and upper part of PTV (z-direction), as can be seen in row (a) for all patients. This implies that the PTV suffers under- and over-dosage due to the interplay effect and dose accumulation, respectively. These effects can be seen in rows (b) and (c) for four out of the five patients: in case 1 there is underdosage in the lower part of the PTV; in case #2 there is overdosage in the lower part of the PTV; in case #3 there is over- and under-dosage in the lower and the upper part of the PTV, respectively; and in case # 4 there is overdosage in the upper part of the PTV. There are relevant uncertainties in cases #2 and #3 over $D_{\mathrm{min},V}$ with variability above 5%. These results are in accordance with Li *et al* (2013) and Zou *et al* (2014), whose authors pointed out that if the original PTV (including the ITV) is used to evaluate a 4D dose distribution, the PTV coverage could suffer significant dosimetric variation. Therefore, we have evaluated 4D doses with the ETV (Azcona *et al* 2019) because this concept is more suitable than PTV to assess 4D dose distributions. PTV has some limitations (Azcona *et al* 2019). By using the ETV in this way for dosimetric comparison, we also isolate the interplay effect more clearly from the accumulation effect. This is an important contribution of this study, because with the ETV we include the uncertainty of the DIR in 4D dose evaluation.

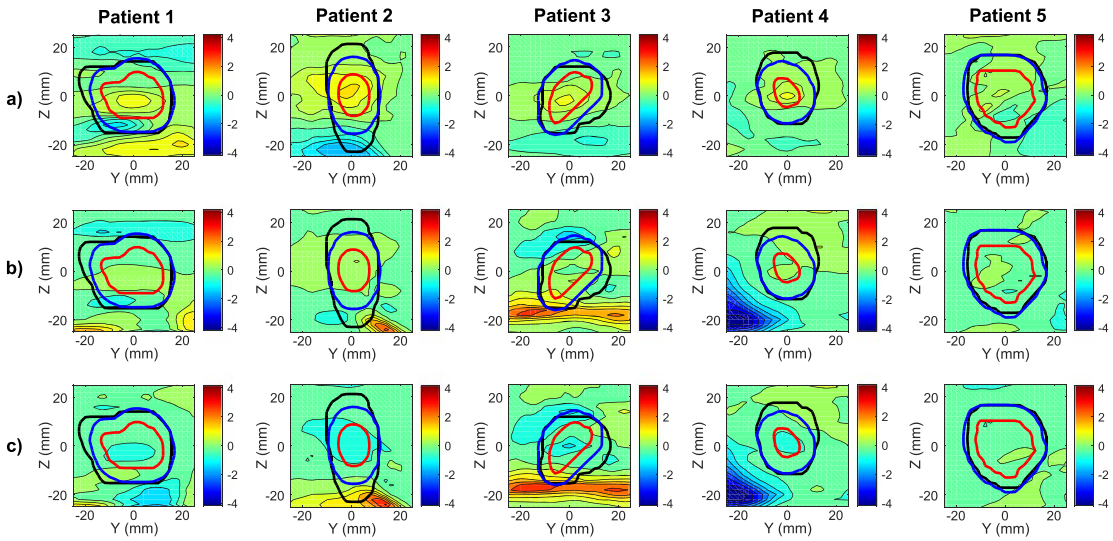

Figure 7. Comparison of 4D dose distributions without taking into account the interplay effect ($\mathcal{D}_{acc}$) and 4D dose distributions obtained through the proposed method ($\mathcal{D}_{acc}^{\max}$ and $\mathcal{D}_{acc}^{\min}$). The GTV is represented in thick red, the PTV in thick black, and the ETV in thick blue. Row (a) shows $\mathcal{D}_{acc}^{\max} - \mathcal{D}_{acc}^{\min}$, row (b) shows $\mathcal{D}_{acc}^{\max} - \mathcal{D}_{acc}$ and row (c) displays $\mathcal{D}_{acc}^{\min} - \mathcal{D}_{acc}$. The differences are shown in Gy units. All plots are in the sagittal plane (Z: superior-inferior direction; Y: anterior-posterior direction), with the GTV split in half by the GTV centroid. Each column corresponds to a different patient.

Focusing now on the ETV, the variability in both indicators (D_{95} and $D_{\min,V}$) was below 2% in all cases, except in case #3, where the variation in $D_{\min,V}$ was 7.4%, due to a cold spot in the GTV by $\mathcal{D}_{acc}^{\min}$. In addition to this, in rows (b) and (c) (figure 7) there are hot and cold spots on the borders outside the ETV in all patients. These hot and cold spots differ spatially depending on whether we are comparing $\mathcal{D}_{acc}^{\max}$ with $\mathcal{D}_{acc}$ (row (b)) or $\mathcal{D}_{acc}^{\min}$ with $\mathcal{D}_{acc}$ (row (c)). The reason for this is that in the procedures for obtaining $\mathcal{D}_{acc}^{\max}$ and $\mathcal{D}_{acc}^{\min}$ the assignment of phases to control points differed. The relevance of overdosage and underdosage is when it occurs in healthy tissue adjacent to the tumor. Our results are in accordance with Zou *et al* (2014), whose authors found differences in a range of ± 5 Gy at the superior and inferior borders outside the PTV. As they explained, due to tumor motion, the upper and lower regions outside the PTV (they used a special PTV modified for evaluating the 4D dose) were in the radiation beam only in some phases of the respiratory cycle. In addition to tumor motion, the respiratory pattern could be another cause behind these hot and cold spots produced just outside the borders of the ETV. Riley *et al* (2014) observed large gamma fail rate within the target region for patients with irregular breathing patterns. In our study, patients 3 and 4, whose ETVs have hot and cold spots of 3 and 4 Gy in adjacent healthy tissue, were recorded to have irregular breathing patterns, with standard deviations of 3.3 seconds and 1 second. In conclusion, if the respiratory pattern is irregular, interplay effect-based dosimetric uncertainty in adjacent healthy tissue or within the target region, can be expected to increase. Yang and Timmerman (2018) pointed out that if the respiratory pattern is highly irregular, the effect of interplay on doses in the target region is not negligible. The implication of these studies is that in lung SBRT, it is important to evaluate a patients breathing pattern. In this work we have approximated the tumor position at any time by the position as represented in the closest 4D CT phase. Moreover, uncertainty in breathing amplitude during treatment is small for most patients (Bissonnette *et al* 2009, Sonke *et al* 2009). Respiratory uncertainty was thus considered by its breathing period. A variation of this method could be performed by using principal component analysis to model lung motion (Cai *et al* 2015).

For clinicians involved in treatment planning, the implementation of the method proposed here would help evaluation and improve quality of treatment for those cases in which this effect could be of concern because of patient's breathing pattern or field size in the control point sequence. It is worth noting that the maximum and minimum potential dose are to some extent hypothetical, but are useful to evaluate the potential effect of interplay once treatment planning is completed. The method quantifies the uncertainty in dose administration, providing oncologists with more information with which to evaluate the quality of treatment.

4.2. Dosimetric uncertainties due to breathing rate

The results shown in figure 4 are consistent with previous studies (Court *et al* 2008, 2010, Ong *et al* 2011, 2013, Stambaugh *et al* 2013, Edvardsson *et al* 2018); which indicate that dosimetric uncertainties due to the interplay effect generally increase with long breathing periods. In both patients studied here, the highest differences between each pair of DVHs occurred in the interval $\left[\frac{f}{4}, f\right]$. Those differences are a consequence of the

assignment of phases to control points. The first panel of figure 5 shows the beam on time (BT) for control points in all patients, sorted in descending order and divided by each patient's breathing period (T). To better illustrate the phase assignment, two horizontal lines have been drawn corresponding to the period of the respiratory cycle (T; dotted line) and the phase time (T_p; discontinuous line). Following the algorithm explained in section II.A.1, we differentiated three cases:

(a) Control points above T are assigned to all phases with a weighting of $\frac{1}{M}$.

(b) Control points that are below T_p, are assigned with to a single phase, with weighting of 1.

(c) Control points that are in the middle zone (above T_p and below T) will be assigned to several phases, each with the corresponding weighting.

In cases (b) and (c) the interplay effect will influence the dosimetric uncertainty. A modification of the breathing rate will modify the number of control points falling into each of the three cases (a)–(c). The third panel of figure 5 displays the range (δ_i) for each control point in each patient, calculated as described in section 2.5.

4.3. Dosimetric uncertainties by the variation of field size

As expected, there is dispersion in the experimental data in figure 6. This variation exists because dosimetric uncertainties due to the interplay effect depend on many variables (including field size, beam-on time, tumor motion). Our data reveal that, as we increase A_{cp} with respect to A_t, the dosimetric uncertainties CV decrease exponentially. It is important to keep in mind that, in our DMPO optimization, we ask to have the control points with area at least of 4 cm^2. All the subsequent results on interplay for our clinical cases should be regarded as having being planned with this constraint, which impacts on the interplay induced uncertainty. A large field size, however, implies less conformation with the tumor volume, and so, in practical clinical terms, the challenge is to find the right compromise in the field size such that uncertainty due to the interplay effect is reduced but precision of tumor coverage is not lost.

5. Conclusion

A method based on 4D accumulation has been developed to quantify dosimetric uncertainties due to the interplay effect. To assign control points to respiratory phases, the method includes some characteristics of a patient's irregular breathing patterns. Tests with the method showed that interplay resulted in uncertainty in GTV of less than 2% but that in some patients it produced uncertainty of potential clinical relevance in PTV. To include DIR uncertainties in 4D evaluation and to identify if hot/cold spots produced through the interplay effect inside or around a tumor were relevant, the method also looked at ETV. ETV takes into account DIR uncertainty, and is more reliable than the PTV for assessment of accumulated 4D dose matrices. In this way, DIR and interplay uncertainties are separated. This work main finding was to reveal, with the proposed methodology, potential and significant dosimetric uncertainty (hot and cold spots) located at the superior and inferior borders outside the ETV. These hot and cold spots resulted from the interplay effect and could be accentuated by irregular breathing patterns. Over- and under-dosages around the borders of the ETV are of clinical importance if there are organs at risk near the ETV. This work analized dose plans built with minimum field size of 4 cm^2; it would be a useful tool to investigate how interplay affects dose distributions tailored using smaller field sizes. The method was also used to show that the uncertainty in mean tumor dose decreases exponentially with increasing field size and increases as breathing rate decreases.

References

Azcona J D, Huesa-Berral C, Moreno-Jiménez M, Barbés B, Aristu J J and Burguete J 2019 A novel concept to include uncertainties in the evaluation of stereotactic body radiation therapy after 4D dose accumulation using deformable image registration *Med. Phys.* **46** 4346–55

Bissonnette J P *et al* 2009 Quantifying interfraction and intrafraction tumor motion in lung stereotactic body radiotherapy using respiration-correlated cone beam computed tomography *Int. J. Radiat. Oncol. Biol. Phys.* **75** 688–95

Bortfeld T, Jiang S B and Rietzel E 2004 Effects of motion on the total dose distribution *Semin. Radiat. Oncol.* **14** 41–51 WB Saunders

Bortfeld T, Jokivarsi K, Goitein M, Kung J and Jiang S B 2002 Effects of intra-fraction motion on IMRT dose delivery: statistical analysis and simulation *Phys. Med. Biol.* **47** 2203–20

Brock K K, Mutic S, McNutt T R, Li H and Kessler M L 2017 Use of image registration and fusion algorithms and techniques in radiotherapy: report of the aapm radiation therapy committee task group no. 132 *Med. Phys.* **44** 43–76

Cai W *et al* 2015 3D delivered dose assessment using a 4DCT-based motion model *Med. Phys.* **42** 2897–907

Court L E, Wagar M, Ionascu D, Berbeco R and Chin L 2008 Management of the interplay effect when using dynamic MLC sequences to treat moving targets *Med. Phys.* **35** 1926–31
Court L *et al* 2010 Evaluation of the interplay effect when using RapidArc to treat targets moving in the craniocaudal or right-left direction *Med. Phys.* **37** 4–11
Edvardsson A, Nordström F, Ceberg C and Ceberg S 2018 Motion induced interplay effects for VMAT radiotherapy *Phys. Med. Biol.* **63** 085012
Keall P J *et al* 2006 The management of respiratory motion in radiation oncology report of AAPM Task Group 76 a *Med. Phys.* **33** 3874–900
Li X, Yang Y, Li T, Fallon K, Heron E and Huq M S 2013 Dosimetric effect of respiratory motion on volumetric-modulated arc therapy-based lung SBRT treatment delivered by TrueBeam machine with flattening filter-free field *J. Appl. Clin. Med.* **14** 195–204
Mutaf Y D, Scicutella C J, Michalski D, Fallon K, Brandner E D, Bednarz G and Huq M S 2011 A simulation study of irregular respiratory motion and its dosimetric impact on lung tumors *Phys. Med. Biol.* **56** 845–59
Netherton T *et al* 2018 Interplay effect on a 6-MV flattening-filter-free linear accelerator with high dose rate and fast multi-leaf collimator motion treating breast and lung phantoms *Med. Phys.* **45** 2369–76
Ong C, Verbakel W F, Cuijpers J P, Slotman B J and Senan S 2011 Dosimetric impact of interplay effect on RapidArc lung stereotactic treatment delivery *Int. J. Radiat. Oncol. Biol. Phys.* **79** 305–11
Ong C L, Dahele M, Slotman B J and Verbakel W F 2013 Dosimetric impact of the interplay effect during stereotactic lung radiation therapy delivery using flattening filter-free beams and volumetric modulated arc therapy *Int. J. Radiat. Oncol. Biol. Phys.* **86** 743–8
Rao M, Wu J, Cao D, Wong T, Mehta V, Shepard D and Ye J 2012 Dosimetric impact of breathing motion in lung stereotactic body radiotherapy treatment using image-modulated radiotherapy and volumetric modulated arc therapy *Int. J. Radiat. Oncol. Biol. Phys.* **83** 251–6
Riley C, Yang Y, Li T, Zhang Y, Heron D E and Huq M S 2014 Dosimetric evaluation of the interplay effect in respiratory-gated RapidArc radiation therapy *Med. Phys.* **41** 011715
Schwarz M, Cattaneo G M and Marrazzo L 2017 Geometrical and dosimetrical uncertainties in hypofractionated radiotherapy of the lung: a review *Phys. Med.* **36** 126–39
Sonke J J, Rosi M, Wolthaus J, Van Herk M, Damen E and Belderbos J 2009 Frameless stereotactic body radiotherapy for lung cancer using four-dimensional cone beam CT guidance *Int. J. Radiat. Oncol. Biol. Phys.* **74** 567–74
Stambaugh C *et al* 2013 Experimentally studied dynamic dose interplay does not meaningfully affect target dose in VMAT SBRT lung treatments *Med. Phys.* **40** 091710
Sterpin E *et al* 2012 Helical tomotherapy for SIB and hypo-fractionated treatments in lung carcinomas: a 4D Monte Carlo treatment planning study *Radiother. Oncol.* **104** 173–80
Wanet M, Sterpin E, Janssens G, Delor A, Lee J A and Geets X 2014 Validation of the mid-position strategy for lung tumors in helical TomoTherapy *Radiother. Oncol.* **110** 529–37
Yang M and Timmerman R 2018 Stereotactic ablative radiotherapy uncertainties: delineation, setup and motion *Semin. Radiat. Oncol.* **28** 207–17 WB Saunders
Zou W *et al* 2014 Dynamic simulation of motion effects in IMAT lung SBRT *Radiat. Oncol.* **9** 225